

Two-dimensional analysis of electrical breakdown in a nonuniform gap between a wire and a plane

K. Ramakrishna,^{a)} I. M. Cohen, and P. S. Ayyaswamy

Department of Mechanical Engineering and Applied Mechanics, School of Engineering and Applied Science, University of Pennsylvania, Philadelphia, Pennsylvania 19104-6315

(Received 18 April 1988; accepted for publication 9 September 1988)

Electrical breakdown of a gap between a wire (modeled as a hyperboloid) and a plane has been investigated numerically by solving the two-dimensional form of the diffusion flux equations for the charged particle number densities and Poisson's equation for the self-consistent electric field. Electron impact ionization, thermal ionization, and three-body recombination have been considered as the charged particle production and loss mechanisms. The electrode surfaces are considered to be absorbing and the initial density of the particles is small, but nonzero. A gap length of 0.5 mm is investigated and the gas medium is air or argon at atmospheric pressure. The temporal development of the profiles of ion and electron number densities, potential and electric field, and current growth on both the electrodes are presented when the applied voltage is 1500 and 2500 V for both positive and negative wires. When the wire is negatively biased, the peaks in the radial distribution of both of the charged particle densities near the wire occur off the axis except during the very early part of the breakdown. With positive polarity, the electron density maximum always occurs on the discharge axis, while for ions it moves away from the axis, later in the transient, due to the reverse particle drift in the electric field from the negative polarity case. The discharge spreads farther out into the ambient (almost two times the gap length) when the wire is negatively biased than with positive polarity. The effect of charge separation on the externally applied electric field is significant at voltages 2500 V and higher. Ionization is greater in argon than in air for a fixed potential difference between the electrodes.

I. INTRODUCTION

A detailed understanding of the events occurring during the initiation of a discharge in a nonuniform gap between a wire (a hyperboloid) and a plane is of fundamental importance. Such discharges are encountered, for example, in the microelectronic interconnection by ball bonding.

Several analytical, numerical, and experimental investigations on discharge initiation are reported in the literature for plane parallel and nonuniform gap geometries.¹⁻⁵ Most of the analytical studies of breakdown use a one-dimensional model and treat parallel plane geometry. The resulting species conservation and electric field equations are numerically solved by the method of characteristics.⁶ A few two-dimensional analyses of breakdown between parallel planes are also available.⁷⁻⁹ Recently, a two-dimensional analysis of small uniform gaps filled with helium and contaminants has been reported using a finite element method.⁹

The existing studies of breakdown in nonuniform gaps treat only the axial development of the discharge. Gap nonuniformity is incorporated into the model by accounting for its effect on the initial potential distribution.^{10,11} Analytical and experimental investigations on breakdown in nonuniform gaps have been reviewed in Refs. 12-15. These reviews show that the streamer growth phase of breakdown follows an initial corona phase. These reviews also show that in the streamer growth models assumptions are made about the physical structure of ionization behind the streamer. They include assumptions about the distribution of the charged

particles and the state of the electric field along the streamer. In order to improve these models, it is necessary to obtain more complete solutions to the equations of particle conservation and Poisson's equation. This enables one to describe accurately the events prior to streamer propagation, thereby avoiding the necessity of several of the assumptions (such as the electron number density distribution behind the streamer) made in the description of the streamer growth.

In nonuniform gaps the radial variations of the charged particle densities and electric field may not be neglected and the problem has to be treated two dimensionally. Here, we report a fully two-dimensional analysis of discharge breakdown in a nonuniform gap between a wire and a plane. We employ the diffusion flux equations for charged particle conservation and Poisson's equation for the self-consistent electric field. Positive ions and electrons are assumed to be the major charge carriers. Upon the application of a sufficiently large potential difference between the electrodes, the stray electrons initially present in the gap are accelerated and cause ionization as described by Townsend's first ionization coefficient. This initiates the breakdown. Thermal ionization and three-body recombination have been accounted for through a parametric treatment of electron and ion temperatures. We consider the electrodes to be nearly perfectly absorbing surfaces. To avoid singular behavior which would unnecessarily complicate the numerical analysis, the electrodes are assumed to have a charged particle density boundary condition N_0 , the ambient density due to background radiation. Since this is very small in comparison to the charged particle densities of interest, the electrodes are near-

^{a)} Present address: IBM Corporation, Endicott, NY 13760.

ly perfectly absorbing. The nonzero densities do simulate a weak reflection or emission from the electrode surface, however.

The governing equations have been numerically integrated, using finite difference methods, to evaluate the spatiotemporal development of the discharge. Results are presented in the form of temporal evolution of electrons and positive ions as a function of the applied potential difference.

The results show that the peaks in radial number density profiles occur away from the discharge axis when the wire is negative. With positive polarity of the wire these peaks occur on the axis for the electrons and off the axis for ions at later times. The discharge is spread out farther into the ambient with negative polarity and is more confined to the region near the axis with positive polarity.

II. GOVERNING EQUATIONS, INITIAL AND BOUNDARY CONDITIONS

Consider a slightly ionized, collision-dominated plasma which is adequately described by the continuum (diffusion flux) conservation equations. These equations are derived in Refs. 16 and 17:

$$\frac{\partial N_c}{\partial t} + \nabla \cdot \Gamma_c = P(N_c) - R(N_c), \quad (1)$$

for electrons where

$$\begin{aligned} \Gamma_c &= -(\mu_c/e)(\nabla p_c + eN_c \mathbf{E}), \\ p_c &= kT_c N_c. \end{aligned} \quad (2)$$

A similar equation can be written for the positive ions. We assume that (i) each specie is in equilibrium with its like particles, and (ii) the charged particles are in equilibrium with the local electric field.¹⁸ Specifically, Kline¹⁸ calculated the actual and equilibrium electron energy near a hyperboloidal pin and found for tip radius r of 3 and 10 μm , the critical distance from the tip, X_{cr} , is 0.35 and 0.55 μm , respectively, beyond which the electron is very close to equilibrium with the electric field. In our calculations, r is 5 μm so X_{cr} is about 0.4 μm . Since our gap is 500 μm , the equilibrium electric field should be a good approximation to within our $Z = 0.999$. Here Z is the nondimensional distance on the axis from the plane to the tip. Z is zero on the plane and one on the tip. Densities are very low this close to the boundary because the electrode is assumed to be nearly perfectly absorbing. The self-consistent electric field \mathbf{E} is given by Gauss' law:

$$\nabla \cdot \mathbf{E} = (e/\epsilon_0)(N_+ - N_c), \quad (3)$$

and the electrostatic potential is

$$\mathbf{E} = -\nabla V. \quad (4)$$

It is estimated that the contribution of the magnetic induction to the electric field is much smaller than the threshold electric field for Townsend's ionization.¹⁹

In the above equations, N is number density, P is volumetric production (ionization) rate, R is volumetric recombination rate, and Γ is particle current density such that

$$I = e \int_S (\Gamma_+ - \Gamma_c) \cdot d\mathbf{S} \quad (5)$$

is the current passed by the discharge, D is the diffusion coefficient, μ is the mobility, and e is the magnitude of charge on a single electron. We consider μ to be independent of electric field E . While it is true that for the range of E/N considered here (10^{-20} – 10^{-16} V m^2), the mobility is field dependent, and the electron energy will vary significantly as electrons gain energy from the field. We believe that, for the short times calculated here, electron impact ionization and two-dimensional electron drift are the dominant effects. We have therefore adopted a simplified model in which mobility and temperature are taken to be constant.

For wire-to-plane discharges, it is appropriate to use prolate spheroidal coordinates²⁰ as in Fig. 1:

$$\begin{aligned} x &= a \sinh u \sin v \cos \phi, \\ y &= a \sinh u \sin v \sin \phi, \\ z &= a \cosh u \cos v, \end{aligned} \quad (6)$$

where x , y , and z are the Cartesian coordinates and u , v , and ϕ are the prolate spheroidal coordinates. In these coordinates, the wire electrode corresponds to $v = v_w$, which is nonzero and needs to be specified, and the planar electrode to $v = \pi/2$. The boundary conditions are specified as follows:

$$\text{on } v = v_w, V = V_w \text{ and } N_+ = N_0, \quad N_c = N_0,$$

$$\text{on } v = \pi/2, V = 0 \text{ and } N_+ = N_0, \quad N_c = N_0,$$

$$\text{on } u = 0, \frac{\partial V}{\partial u} = 0 = \frac{\partial N_{+,c}}{\partial u}$$

(this is the axial symmetry condition),
(7)

and

$$\text{as } u \rightarrow \infty, \frac{\partial V}{\partial u} \rightarrow 0, \text{ and } N_+, N_c \rightarrow N_0.$$

The initial number densities of the charged particles are small (but nonzero) due to the omnipresent background radiation. The initial electric field is divergence free and is given by

$$V = V_w \ln[\tan(v/2)] / \ln[\tan(v_w/2)]. \quad (8)$$

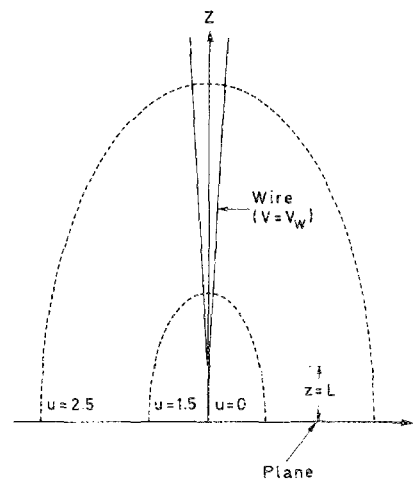


FIG. 1. Schematic diagram of the prolate spheroidal coordinate system for the study of electrical breakdown between a wire and a plane.

A. Modeling of ionization and recombination mechanisms

Electron impact ionization is the main source of the charged particles during the breakdown period and its rate is given by

$$P(N_e) \big|_{\text{impact ionization}} = \alpha_i \mu_e E N_e. \quad (9)$$

The primary ionization coefficient α_i is a function of the ratio of electric field to the gas pressure E/p as given by

$$\alpha_i/p = A_i \exp[-B_i/(E/p)], \quad (10)$$

where the constants A_i and B_i depend on the type of gas under consideration.²¹⁻²⁴ As the breakdown proceeds when the electron temperature increases significantly, thermal ionization (Saha equation) and three-body recombination occur. The net ionization in this situation is given by

$$\begin{aligned} P(N_e) - R(N_e) \big|_{\text{thermal and 3-body}} \\ = \gamma(T_e) N_e \left[\frac{2g_i N_n}{g_n} \left(\frac{2\pi m_e k T_e}{h^2} \right)^{3/2} \right. \\ \left. \times \exp\left(-\frac{eV_i}{kT_e} \right) - N_e N_+ \right], \quad (11) \end{aligned}$$

where h is Planck's constant, k is Boltzmann's constant, g_i is the statistical weight of the ions, g_n is the statistical weight of the ground state of the neutral particles, m_e is the mass of an electron, V_i is the ionization potential of the ground state,

and the recombination coefficient γ_e is a function of electron temperature²⁵:

$$\gamma(T_e) = 1.09 \times 10^{-20} T_e^{-9/2} \text{ (m}^6/\text{s)}. \quad (12)$$

In addition, attachment, detachment, and charge transfer processes are important contributors to ionization in air. However, in the region of large E/N_n , near the wire, electron impact ionization is still the dominant ionization mechanism. Detailed calculations including negative ion reactions were carried out in Chap. 3 of Ref. 19. The results were that the effect of negative oxygen ions were negligible during the early phases of breakdown and, at later times, the negative ions caused a net loss of electrons from the discharge. This effect is most pronounced away from the discharge axis, where the electron densities are the highest. The radial spread of the discharge is relatively unaffected by the presence of the negative ions. The current rise is also unaffected by the negative ions during the early part of the breakdown and the current levels are lower when the negative ions are present.

B. Normalization of governing equations

In seeking appropriate dimensionless formulations, we have found four time scales for the breakdown process. They are

$$\begin{aligned} t_0 &= 1/(A_i p \mu_e E_R) \approx 10^{-9} \text{ s—ionization or initial breakdown time,} \\ t_1 &= L^2/(\mu_e |V_w|) \approx 10^{-9} \text{ s—electron drift time,} \\ t_2 &= d^2 e/(k T_e \mu_e) \approx 10^{-7} \text{ s—electron diffusion time,} \\ t_3 &= d^2 e/(k T_i \mu_i) \approx 10^{-2} \text{ s—ion diffusion time,} \end{aligned} \quad (13)$$

where d is the wire diameter (defined as twice the tip radius of curvature of the hyperboloid), L is the gap length (axial distance between the tip of the hyperboloid and the plane), and E_R is a reference electric field. The numerical values indicated in Eq. (13) are evaluated for air at atmospheric pressure with a wire diameter of 25 μm and a gap length of 500 μm (typical of the ball bonding process used in microelectronic interconnection). Temperatures are normalized by the ambient temperature, T_∞ . The number densities are

normalized using a number density which results in a Debye length equal to the wire diameter and is given by

$$N_R = k T_\infty \epsilon_0 / e^2 d^2. \quad (14)$$

The potential and the electric field are normalized by

$$V_R = k T_\infty / e \text{ and } E_R = V_R / d. \quad (15)$$

The dimensionless governing equations are given by the following: for electrons,

$$\begin{aligned} \frac{\partial n_e}{\partial t'} + \frac{F_e}{(\sinh^2 u + \sin^2 v)} \left[\frac{1}{\sinh u} \frac{\partial}{\partial u} \left(\sinh u n_e \frac{\partial \psi}{\partial u} \right) + \frac{1}{\sin v} \frac{\partial}{\partial v} \left(\sin v n_e \frac{\partial \psi}{\partial v} \right) \right] \\ = \frac{F_e T_e'}{(\sinh^2 u + \sin^2 v)} \left[\frac{1}{\sinh u} \frac{\partial}{\partial u} \left(\sinh u \frac{\partial n_e}{\partial u} \right) + \frac{1}{\sin v} \frac{\partial}{\partial v} \left(\sin v \frac{\partial n_e}{\partial v} \right) \right] \\ + e^{-B/E'} n_e E + C_1 C_2 n_e T_e'^{-3} e^{-\psi/T_e'} - C_1 T_e'^{-9/2} n_e^2 n_+, \quad (16) \end{aligned}$$

and for potential,

$$\begin{aligned} \frac{1}{(\sinh^2 u + \sin^2 v)} \left[\frac{1}{\sinh u} \frac{\partial}{\partial u} \left(\sinh u \frac{\partial \psi}{\partial u} \right) \right. \\ \left. + \frac{1}{\sin v} \frac{\partial}{\partial v} \left(\sin v \frac{\partial \psi}{\partial v} \right) \right] = \frac{a^2}{d^2} (n_e - n_+), \quad (17) \end{aligned}$$

where

$$\begin{aligned} n &= \frac{N}{N_R}, \quad \psi = \frac{V}{V_R}, \quad T' = \frac{T}{T_\infty}, \quad E' = \frac{E}{E_R}, \\ F_e &= \frac{\mu_e V_R t_0}{a^2}, \quad F_+ = \frac{\mu_+ V_R t_0}{a^2}, \end{aligned}$$

$$\begin{aligned}
t_0 &= 1/(A_i \rho \mu_c E_R), \quad t' = t/t_0, \\
C_1 &= 1.09 \times 10^{-20} N_R^2 T_\infty^{-9/2} t_0, \\
C_2 &= 4.8186 \times 10^{21} N_n g_i T_\infty^{3/2} / (N_R^2 g_n), \\
N_n &= \text{neutral density}.
\end{aligned}
\tag{18}$$

The dimensionless form of the ion equation and the limiting form of the governing equations near $u = 0$ have been omitted for brevity and the details may be found in Ref. 19.

III. NUMERICAL SOLUTION

The salient features of the numerical solution are: (1) implicit time integration, (2) central differences for the discretization of diffusion terms, and (3) an upwind difference method is employed for the drift terms.²⁶ In an upwind method a combination of forward and backward differences is used for drift terms depending upon the sign of the charge on the particle and the direction of the local electric field. The algebraic equations resulting from the discretization of the governing equations are solved using the line-by-line method along with the computationally efficient Thomas (tridiagonal) algorithm. The development of the numerical solution is presented in Ref. 19.

IV. RESULTS AND DISCUSSION

Numerical solutions for electrical breakdown in air and argon have been obtained for negative and positive polarities of the wire with applied voltages in the range of 1200–5000 V. Here we choose to present results for 1500 and 2500 V and the results for the remaining voltages will be available in Ref. 19. A gap length of 0.5 mm (20 mils) and $v_w = 0.1$ have been used in all of the computations. The tip radius of the wire is taken to be the radius of curvature of the hyperboloid of revolution with $v_w = 0.1$ and has a value of 0.01 mm. These geometric parameters are typical of the ball bonding process used in microelectronic interconnection. The ambient pressure and temperature are 1 atm and 500 K, respectively. Electron temperature T_e is fixed at 5000 K. Results of computations with $T_e = 2000$ K are only slightly different from the breakdown characteristics at 5000 K. The initial density of the charged particles N_0 is taken to be $6 \times 10^8 \text{ m}^{-3}$ and is from Ref. 27. The parameters used in the calculations are listed in Tables I and II.

TABLE I. Parameters used for air and argon.

Type of gas	Air	Argon
A_i (m/N)	6.5 (Ref. 21)	9.0
B_i (V m/N)	191	135
μ_c ($\text{m}^2/\text{V s}$)	0.0348	0.019
Threshold electric field		
E_0 (V/m)	2.28×10^6	3.8×10^5
t_0' (s)	1.02×10^{-8}	1.35×10^{-8}

TABLE II. Reference data.

$N_0 = 6 \times 10^8 \text{ m}^{-3}$ (Ref. 26)
$N_n = 1.47 \times 10^{25} \text{ m}^{-3}$
$N_R = 2.36 \times 10^{16} \text{ m}^{-3}$
$p = 760 \text{ Torr} = 101\,325 \text{ N/m}^2$
$T_\infty = T_i = 500 \text{ K}$
$T_e = 5000 \text{ K}$
$L = 0.5 \text{ mm}$
$d = 0.01 \text{ mm}$
$V_R = 0.043 \text{ V}$
$E_R = 4287 \text{ V/m}$
$I_R = 2.85 \times 10^{-9} \text{ A}$
$E/N_n: 2 \times 10^{-18} - 4 \times 10^{-17} \text{ V/m}^2$ (2000–40000 Td)

A. Negative wire

1. Number density growth on the axis

Figure 2 shows the temporal variation of the electron and ion number densities in air at several locations on the discharge axis when the wire is negatively biased with respect to the planar electrode, viz., $V_w = -2500$ V. We notice that at any given location, the number densities of the charged particles precipitously rise from the initial value (2.54×10^{-8}) by several decades (as many as 10 decades at some locations). This rise in number densities occurs at progressively later times for locations farther from the wire tip as the ionization wave travels from the wire to the plane. In the regions of intense electric field near the wire, at $Z = 0.99$ (where $Z = z/L$), the increases in the number densities of the electrons and the ions are mainly due to their production by ionization. There is very little drift even of the electrons at these locations as the time is too short for drift to set in. For this reason, the curves for electrons and ions at these locations are virtually coincident. However, further from the wire, at $Z = 0.8, 0.67$, or 0.36 , we notice that the rise in the

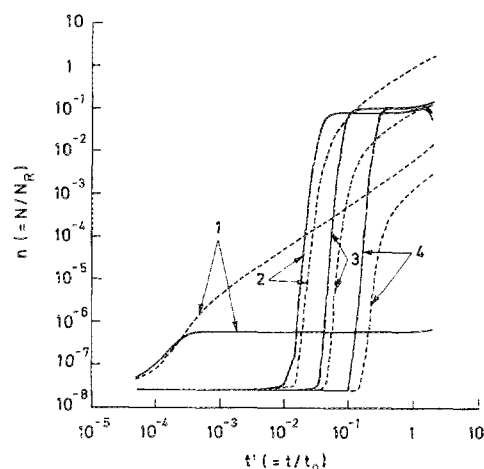


FIG. 2. Temporal development of the electron and ion number densities in air at several locations on the discharge axis with the wire at -2500 V. $T_\infty = 500$ K, $p = 760$ Torr, $L = 5 \times 10^{-4}$ m, and $d = 10^{-5}$ m. $Z = z/L$, $N_R = 2.36 \times 10^{16} \text{ m}^{-3}$, $N_n = 1.47 \times 10^{25} \text{ m}^{-3}$, and $t_0 = 1.02 \times 10^{-8}$ s. Legend: solid lines, electron number density, dashed lines, ion number density, (1) $Z = 0.99$, (2) $Z = 0.80$, (3) $Z = 0.67$, (4) $Z = 0.36$.

number density of electrons leads (in time) that of the ions. The electrons, which are at first copiously produced near the wire, drift to locations away from the wire (towards the planar electrode). This explains the initial rise noted in their density at these locations. After sufficient buildup at further locations from the wire, the electrons cause ionization there, producing the ions. In turn, we notice a precipitous rise in ion density. In this connection we may note that the volumetric impact ionization rate, the main mechanism for particle production, is proportional to the *product* of the electron number density and the local electric field, viz., $n_e E$. Similar observations are also made with V_w in the range of -1200 V to -5000 V and the number density levels increase with increasing voltage.

Following the steep rise, the electron number densities level off while the ion densities continue to increase with time. Since electrons are more mobile than ions, they drift towards the planar electrode (anode) following their production. In the brief time considered here, the heavier ions stay nearly immobile at the location of their production with consequent continued increase in density.

Figure 3 shows similar results for argon when the wire is negative with respect to the planar electrode and is biased to -1500 V. The number densities are higher for argon than for air for a fixed potential difference between the electrodes. This is due to a higher impact ionization coefficient for argon for the same value of E/p .

2. Number density profiles on the axis

In Fig. 4 the number density profiles on the discharge axis are shown at different times during the transient in air with $V_w = -2500$ V. For $t' < 7.5 \times 10^{-4}$ the ionization is localized near the wire. For $t' > 0.8$ the profiles of the electron density become invariant with time as their volumetric production rate is balanced by their loss to the anode. On the other hand, the ion number densities continue to increase with time as their loss from the discharge to the cathode (wire) is smaller than the production rate mainly due to smaller drift.

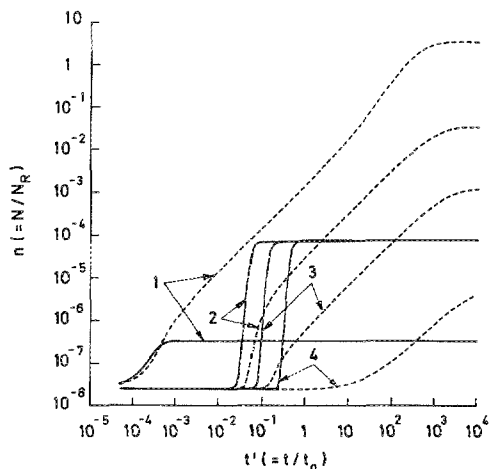


FIG. 3. Temporal development of the electron and ion number densities in argon at several locations on the discharge axis with the wire at -1500 V. $T_w = 500$ K, $p = 760$ Torr, $L = 5 \times 10^{-4}$ m, and $d = 10^{-5}$ m. Legend: (1) $Z = 0.99$, (2) $Z = 0.80$, (3) $Z = 0.67$, (4) $Z = 0.36$.

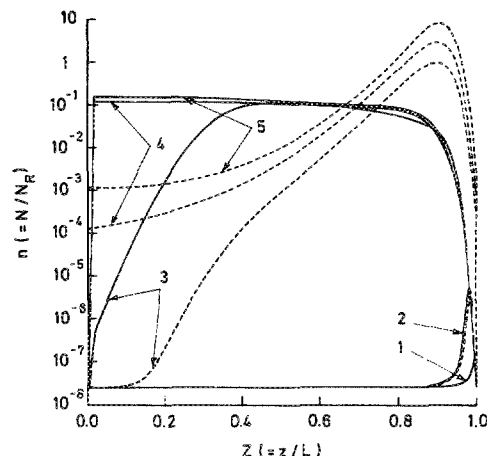


FIG. 4. Axial number density profiles of electrons and ions in air at several times during the transient with the wire at -2500 V. Legend: (1) $t' = 10^{-4}$, (2) $t' = 7.5 \times 10^{-4}$, (3) $t' = 0.3$, (4) $t' = 0.8$, (5) $t' = 1.9$.

While the peaks in the profiles of electron density move from the cathode (wire) to the anode (plane) throughout the transient, the peaks in ion number density profiles move along with the peaks of the electron density, towards the anode, during the earlier portion of the transient ($t' < 7.5 \times 10^{-4}$) and towards the cathode at later times. During the initial portion of the breakdown the electron-ion pairs produced due to ionization stay together and at later times the ions move towards the cathode as their drift motion sets in. Even early in the transient, the peak of the electron number density leads the peak of the ion density as the electron drift sets in earlier than ion drift.

Beyond $t' = 1.9$ in Fig. 4, the present numerical formulation does not converge and more sophisticated schemes may have to be employed. We believe that the lack of convergence is due to the following reasons: (i) Development of regions of severe gradients adjacent to the walls (sheaths) in the solution domain; with higher applied voltages this occurs at earlier times. (ii) Alternatively, we notice that the solution algorithm fails when charge neutrality is nearly achieved with consequent small Debye length (large n_e, n_i) in the central portion of the discharge. Poisson's equation cannot then be integrated for the potential because the space charge becomes a small difference between two large nearly equal number densities. However, with -1500 V, convergence is obtained for $t' = 10000$ and this corresponds to a dimensional time of the order 10^{-4} s. At this voltage, ionization is insufficient to decrease the Debye length to the point where convergence becomes problematic.

3. Radial profiles of the number densities

Figure 5 shows radial profiles of number densities of electrons and ions at a fixed axial location Z of 0.99, in air at different times during the breakdown with $V_w = -2500$ V. Initially the maximum value of both number densities occurs on the discharge axis, $r = 0$. As the breakdown progresses, the peaks in radial number density profiles move off the axis. When the wire is negative, the radial component of the electric field, $E_r = -\partial\psi/\partial r$, is directed towards the

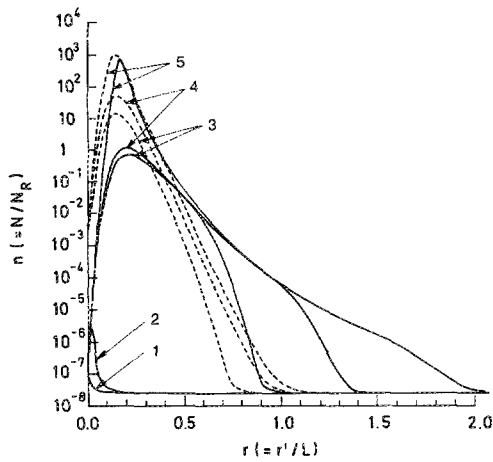


FIG. 5. Evolution of the radial number density profiles of electrons and ions in air with the wire at -2500 V, $Z = 0.99$. Legend: (1) $t' = 10^{-4}$, (2) $t' = 7.5 \times 10^{-4}$, (3) $t' = 0.3$, (4) $t' = 0.8$, (5) $t' = 1.9$.

axis, i.e., it is radially inward. (Refer to the radial profile of the potential distribution in Fig. 6.) As the electrons drift in the direction opposite to the local electric field, they move away from the axis at a rate proportional to the product $n_e E_r$. Initially, n_e and the drift flux are small and the peaks occur on the axis. As time progresses, at any fixed location, the electron number density increases due to both increased drift flux and due to impact ionization. We note also that densities are depressed very close to the wire because of the absorbing wall boundary condition. This requires the diffusive flux to dominate over the drift at the wall. These factors contribute to the electron number density peak occurring away from the axis as time increases, when the wire is negative. The electrons that drift away from the discharge axis cause ionization after sufficient buildup of their number density away from the axis. This is necessary as the electric field decreases radially outward and the local volumetric ionization rate is proportional to the product, $n_e E$. The peak in the radial ion number density profile also occurs off the axis, when the wire is negative, as the production of ions depends upon the local electron density. Even though the ion drift is towards the axis, the ion number density still peaks away

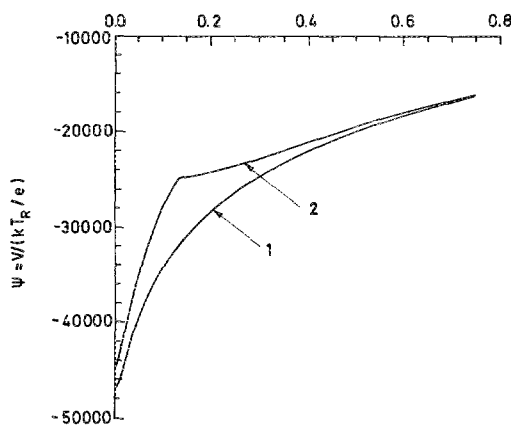


FIG. 6. Radial profiles of the potential in air at two times during the transient with the wire at -2500 V, $Z = 0.99$. Legend: (1) $t' = 0$, (2) $t' = 1.9$.

from the axis as the ion drift is much slower than the electron drift. It is seen here that the ion peaks shift towards the axis and electron peaks away from it. This effect may be observed more clearly with $V_w = -1500$ V as we could integrate the equations for longer times.

The disparity in the time scales of ion and electron drift mechanisms is evident from their relative spread away from the axis. In Fig. 5 the ion distribution is confined to a narrower region ($r < 1.15$) than that of the electrons ($r < 2.0$). It may be noted that the radial coordinate is normalized with respect to the gap length. As the radial distance from the axis increases, the radial component of the electric field decreases and with it the production of the charged particles. Beyond $r = 1.15$, a higher electron number density may be attributed to electron drift at higher rates than the ions from the regions of higher densities.

In Fig. 5 we also note that to the left of the peaks in the densities of the particles there is a region ($0.15 < r < 0.4$) of charge neutrality at later times and the densities of both the charged particles are large (between 1 and 1000).

Figure 7 shows the radial profiles of the number densities of the charged particles further from the wire at $Z = 0.67$. This location is just within the ionization front, an envelope surrounding the wire. Inside of this ionization front the magnitude of the local electric field is greater than the threshold electric field, E_0 . Below the threshold electric field Townsend's first ionization coefficient is nearly zero. The number densities at $Z = 0.67$ are smaller than their respective values near $Z = 0.99$ and the space charge, $(n_+ - n_-)$, is smaller at $Z = 0.67$ than at $Z = 0.99$ because the densities at this location are much smaller (by 10^4). The radial spread of the electrons and ions is the same as it is at $Z = 0.99$.

4. Development of profiles of potential distribution and electric field on the discharge axis

Figures 8 and 9 show the development of the potential distribution and the electric field, respectively, on the discharge axis in air when the wire is at -2500 V. The potential distribution does not show any effects of charge separa-

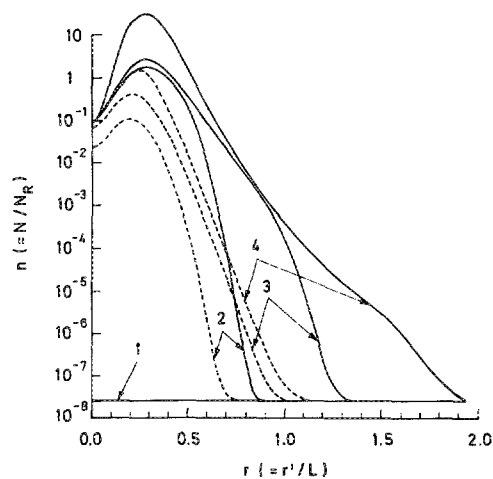


FIG. 7. Evolution of the radial number density profiles of electrons and ions in air with the wire at -2500 V, $Z = 0.674$. Legend: (1) $t' = 7.5 \times 10^{-4}$, (2) $t' = 0.3$, (3) $t' = 0.8$, (4) $t' = 1.9$.

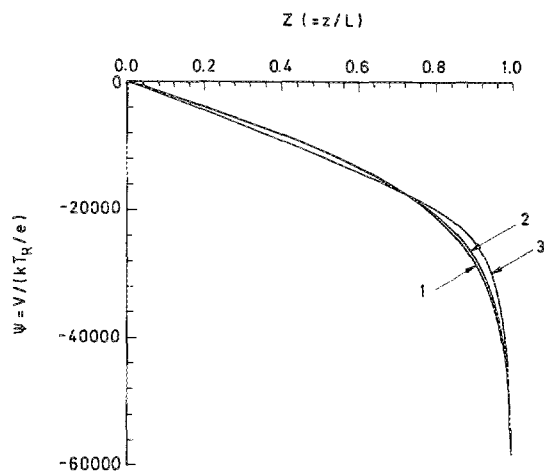


FIG. 8. Development of electrostatic potential on the discharge axis in air with the wire at -2500 V. Legend: (1) $t' = 0$, (2) $t' = 0.8$, (3) $t' = 1.9$.

tion for $t \leq 0.3$ and the field is divergence free. At later times, $t \geq 0.8$, the externally applied field is altered by the charge separation established during the breakdown. The effect of charge separation is such that the electric field in the central portion of the discharge axis, viz., $0.46 < Z < 0.96$, decreases from its initial value and it increases near the anode, $Z < 0.46$ as seen from Fig. 9. A small amount of field enhancement near the wire (cathode) is also present. These trends in the temporal development of the electric field on the discharge axis have also been noted in the one-dimensional analyses of breakdown in parallel plane gaps^{11,28,29} and a one-dimensional analysis in nonuniform (two-dimensional) gaps.³⁰ Our computations also show that space charge modifies the electric field over a region in the central part of the discharge during the time interval $0.8 \leq t \leq 1.9$. The effect of the charge is to decrease the externally applied electric field in the central portion of the axis and to increase it near the electrodes. This accelerates the breakdown process. With $V_w = -1500$ V, the electric field remains nearly divergence free during the transient. Charge separation has a negligible effect on the externally applied field. Towards the end of the

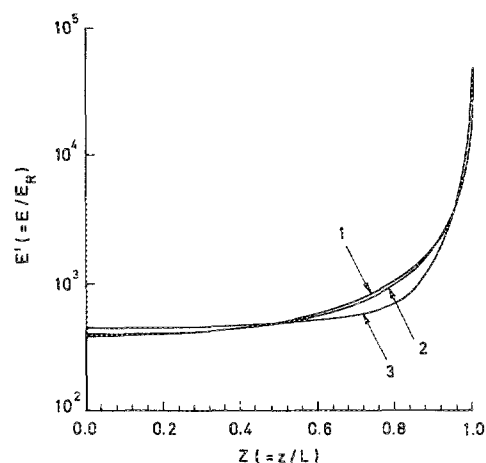


FIG. 9. Development of electric field on the discharge axis in air with the wire at -2500 V. Legend: (1) $t' = 0$, (2) $t' = 0.8$, (3) $t' = 1.9$.

transient, around $t = 10\,000$, the effects of charge separation appear near the wire (cathode) and are very small.

5. Development of radial profiles of potential distribution and electric field

Figures 6 and 10 show temporal development of the potential distribution and the total electric field evolution in the radial direction. At $t' = 1.9$, both the distributions show effects of charge separation with significant variation from its divergence free nature at $t' = 0$. However, such effects are confined close to the axis. The maximum deviation in the potential is at $r = 0.12$, which corresponds to a charge separation of approximately $2 \times 10^{19} \text{ m}^{-3}$. The electric field between the axis and $r = 0.12$ is enhanced by the ionization, while it decreases below its initial value beyond this location. Beyond the quasi-neutral region, the potential distribution and the electric field have not changed appreciably from their initial distributions.

6. Current growth

Figure 11 shows the electron, ion, and total nondimensional current at the cathode (wire) and anode during the transient in air for an applied voltage of -2500 V. Nearly all of the current is from the electrons at both the electrodes. The magnitude of the current at the anode is generally higher than the current at the wire (cathode). The current is almost zero until $t' = 0.4$ and beyond this time current at both electrodes begins to increase. This current rise, which is very rapid at the anode, is by nearly six decades and may be associated with the arrival of the ionization wave at the anode. Meanwhile ion current at the anode, though small compared to electron current, also increases by three decades and is directed away from the anode. Beyond $t' = 0.4$, the ion current gradually increases with time. The current growth for -1500 V is less dramatic than that for -2500 V. At the anode the electron current is very small at first, then it increases by a decade in a very short time and remains constant for the rest of the transient. The ion current to the cathode (wire) increases by several decades from $t' = 1$ to

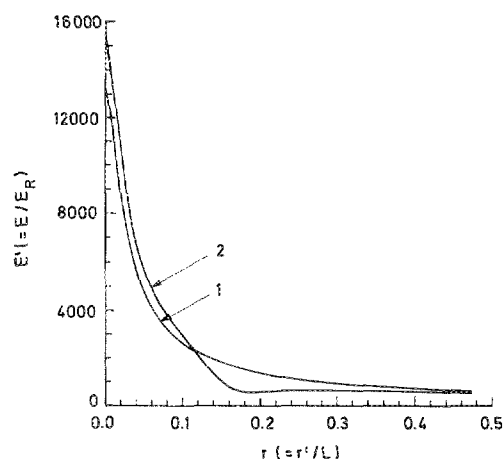


FIG. 10. Development of the radial profile of the electric field in air with the wire at -2500 V. Legend: (1) $t' = 0$, (2) $t' = 1.9$.

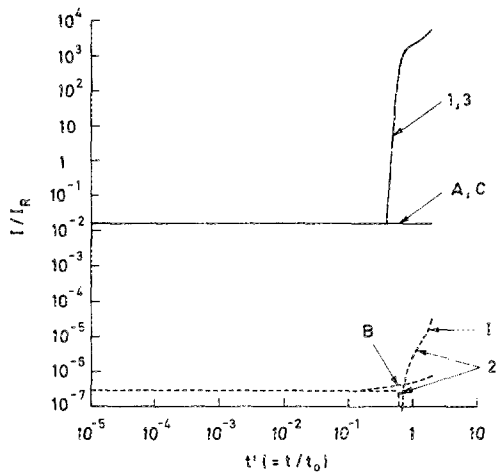


FIG. 11. Nondimensional currents—electronic, ionic, and total—in air at the wire and the plane with the wire at -2500 V. Normalization current $= 2.8 \times 10^{-9}$ A. Legend: Currents at the plane: (1) electron, (2) ion, and (3) total. Currents at the wire: (A) electron, (B) ion, and (C) total. $I \rightarrow$ currents on this portion of the curve are negative.

1000 and reaches a steady value. Even then it is a decade smaller than the electron current.

B. Effect of wire polarity—positive wire

In this section we study the effect of polarity reversal on the discharge development. We note that when the wire is positive, the anode is in the region of intense electric field.

1. Number density growth on the axis

Figure 12 shows temporal variation of electron and ion number densities in air at several locations on the discharge axis when the wire is the anode at a potential of $V_w = 2500$ V. The number densities of both types of charged particles increase gradually unlike that for the negative polarity case where the rise is quite steep (Fig. 2). The growth rate of number density is smaller than in the case of negative polarity and the corresponding number densities are also lower.

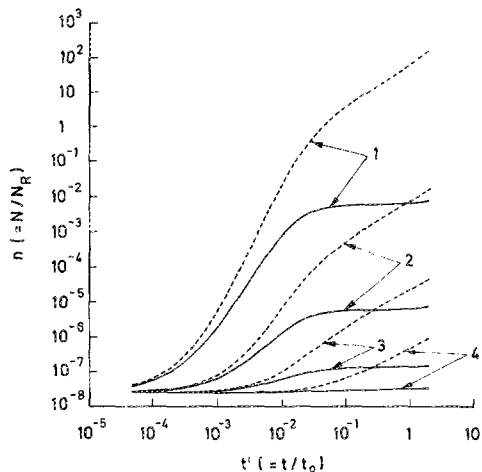


FIG. 12. Temporal development of the electron and ion number densities in air at several locations on the discharge axis with the wire at $+2500$ V. Legend: (1) $Z = 0.99$, (2) $Z = 0.95$, (3) $Z = 0.90$, (4) $Z = 0.80$.

The ionization region is confined closer to the wire as evidenced by the fact that the number densities at locations $Z < 0.9$ are nearly at their initial values. When the wire is positive, the anode (wire) is in a region of intense electric field and that helps keep the electrons (produced by impact ionization near the wire) closer to the wire. In the case of negative polarity, the electrons produced near the wire (cathode) drift away from it, towards the anode (plane), and cause ionization in their wake. This results in a more diffuse discharge in case of negative polarity. On the other hand, with positive polarity the electron densities have reached a plateau, becoming higher when closer to the wire, opposite to the trend observed with negative polarity. Figure 13 shows the same quantities for 1500 V. We note that the ion densities at all locations, wherever buildup of charged particles is present, subsequently reach the same plateau at longer times (~ 3 in Fig. 13). Even at $t' = 10\,000$ with this voltage, ionization has not yet reached $Z = 0.36$.

2. Number density profiles on the axis

The discharge remains quite close to the (positive) wire. The ions move farther (on the axis) from the wire than the electrons due to their drift away from the wire (anode).

3. Radial profiles of the number densities

Figures 14 and 15 show radial profiles of electron and ion densities, at $Z = 0.99$, in air with the wire at 2500 and 1500 V, respectively. In contrast with the negative polarity situation, the charged particle density peaks occur on the axis for all times calculated at 2500 V. However, at 1500 V, the peak in the ion density occurs on the axis during the earlier portion of the transient and moves away from the axis for $t' > 3.95$ (Fig. 15). These results may again be explained by considering the direction of particle drift in the electric field. With the positive wire, the radial component of the electric field is directed away from the axis causing electrons to drift towards the axis and the ions away from it. This in turn causes the electron density peak to occur on the axis and

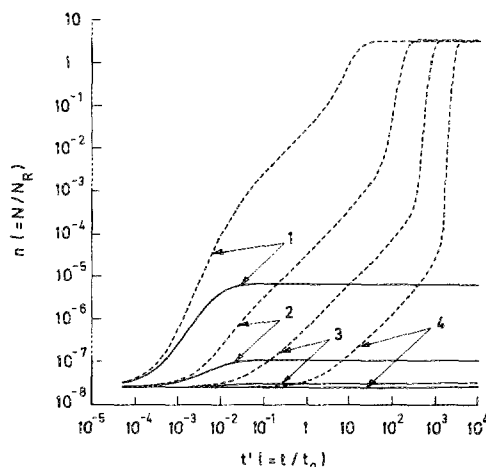


FIG. 13. Temporal development of the electron and ion number densities in air at several locations on the discharge axis with the wire at $+1500$ V. Legend: (1) $Z = 0.99$, (2) $Z = 0.95$, (3) $Z = 0.90$, (4) $Z = 0.80$.

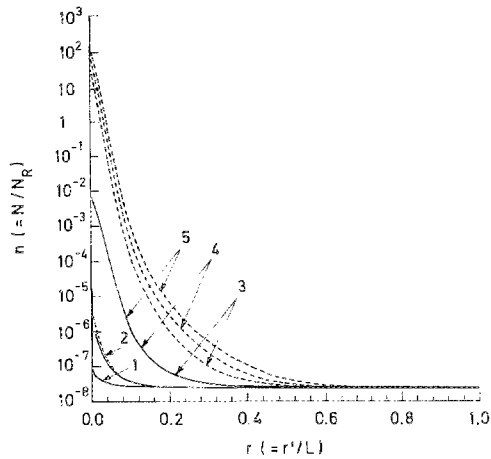


FIG. 14. Evolution of the radial number density profiles of electrons and ions in air with the wire at +2500 V, $Z = 0.99$. Legend: (1) $t' = 10^{-4}$, (2) $t' = 7.5 \times 10^{-4}$, (3) $t' = 0.3$, (4) $t' = 0.8$, (5) $t' = 1.8$.

the ion peaks to drift away from the axis. As the ionic drift is slower, the peak moves away from the axis at later times. For the same reason, the radial spread of ions is smaller for positive polarity ($r < 0.6$ in Figs. 14 and 15) as compared with negative polarity ($r < 2$ in Fig. 5).

4. Electric field on the discharge axis

The potential distribution remains mainly at its initial distribution and charge separation effects are negligible for 1500 and 2500 V.

5. Current growth

The current growth curves for 2500 V, Fig. 16, exhibit the same general features as discussed for negative polarity, such as higher current at the anode (wire) and electron current being greater than ion current. However, the current growth curves for positive polarity show some important differences from their negative polarity counterparts. Ion current at the anode begins to increase simultaneously with the increase of electron current to the anode and this ion

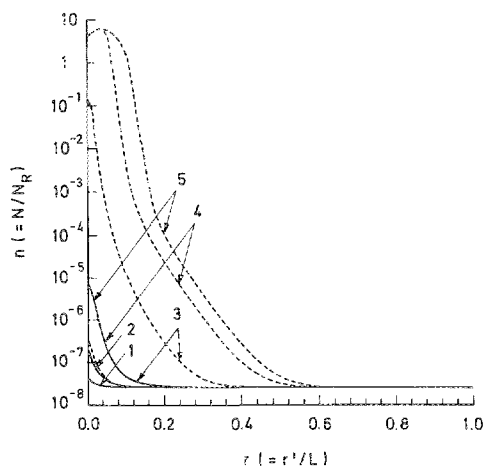


FIG. 15. Evolution of the radial number density profiles of electrons and ions in air with the wire at +1500 V, $Z = 0.99$. Legend: (1) $t' = 10^{-4}$, (2) $t' = 7.5 \times 10^{-4}$, (3) $t' = 0.3$, (4) $t' = 0.8$, (5) $t' = 1.8$.

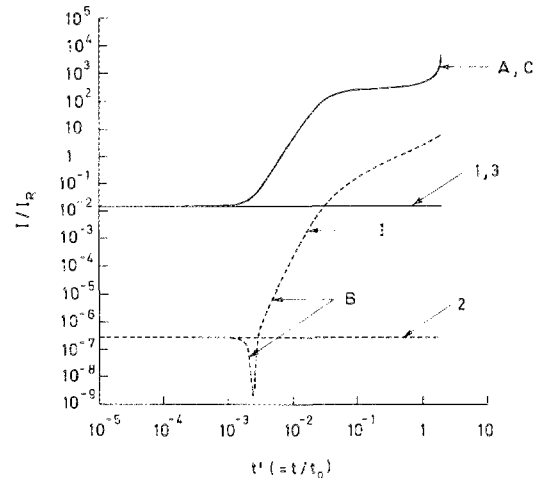


FIG. 16. Nondimensional currents—electronic, ionic, and total—in air at the wire and the plane with the wire at +2500 V. Normalization current = 2.8×10^{-9} A. Legend: Currents at the plane: (1) electron, (2) ion, and (3) total. Currents at the wire: (A) electron, (B) ion, and (C) total. $I \rightarrow$ currents on this portion of the curve are negative.

current near $t' = 1$ is about a decade smaller than the electron current. The larger ionic current at the anode, with positive polarity, appears to be due to the larger electric field experienced by the ions in the anode (wire) region as compared with the negative polarity case when the anode is planar. The larger electric field near the wire results in a larger drift flux and thus current of ions. The electron current to the anode is nearly zero at first and it begins to increase (less rapidly than in the case of negative wire), reaching a plateau (approximately between $0.1 < t < 1.0$), and then increases very rapidly near $t' = 1.8$. This trend is similar to the negative polarity case except the initial rise is more rapid and the plateau less noticeable with negative polarity.

With 1500 V applied to the wire, electron motion contributes entirely to the total current at the anode (wire). It increases by a small amount (about two times) over a short period of time and reaches a constant value for the remainder of the transient period. There is no current at the cathode for the entire duration ($t = 10\,000$) of the transient as the ionization has not yet reached the planar electrode.

V. CONCLUSIONS

Electrical breakdown characteristics of air or argon at atmospheric pressure in a nonuniform gap between a wire and a plane have been studied numerically by solving the two-dimensional form of the diffusion flux equations for the charged particle number densities and Poisson's equation for the self-consistent potential. Electrons initially present from background radiation initiate the breakdown. Electron impact ionization, thermal ionization, and three-body recombination are employed for the charged particle production and loss mechanisms. The electrode surfaces are considered to be absorbing. A gap length of 0.5 mm is used. The temporal development of the axial and radial profiles of ion and electron number densities, potential and electric field, and current growth on both the electrodes are presented

when the applied voltage is 1500 and 2500 V for both positive and negative wires. From this study we may conclude:

(1) The discharge spreads further out into the ambient when the wire is negatively biased than with positive polarity.

(2) When the wire is negatively biased, the peaks in the radial profiles of both the charged particle densities near the wire occur away from the axis except during the early part of the breakdown. With positive polarity, electron density maxima occur on the discharge axis, while for ions they move away from the axis later in the transient due to particle drift in the electric field.

(3) With the applied voltage at -2500 V, charge separation causes a decrease in the electric field in the middle of the discharge and an increase near the electrodes as compared with the externally applied field. However, the effects of charge separation are negligible for voltages below 1500 V.

(4) At 2500 V, current growth is very rapid at the anode (nearly six decades and is of order 10^{-5} A at its peak). The current growth with 1500 V is less dramatic than for 2500 V. Ion current away from the anode, even though small compared to electron current, also increases by three decades or more for 2500 V. Current variation with time is steeper with negative polarity than with positive polarity.

(5) Corresponding results in argon from Ref. 19 show that the voltages necessary to achieve a given level of ionization with argon are lower than for air. (See also Fig. 3.)

(6) At lower voltages, in the neighborhood of 400 V for air, the computations show that current and number densities are very small with the results that the gap is essentially nonconducting.

ACKNOWLEDGMENTS

This material is based upon work supported by the National Science Foundation under Grant No. DMC 8513128. Numerical computations were made possible under the NSF Supercomputer Grant No. DMC 0000000/8513128 and have been performed mostly on the Cray-X/MP-48 at the Pittsburgh Supercomputer Center. Some support was also provided by the Advanced Technology Center of Southeastern Pennsylvania under the Benjamin Franklin Partnership Program, Grant No. 06.500NU. The authors also would like

to thank Professor J. Dutton of the University of Swansea, United Kingdom and Professor Eric E. Kunhardt of the Weber Research Institute, Polytechnic University, Brooklyn, New York for many helpful discussions and encouragement.

- ¹F. Llewellyn-Jones, *Ionization and Breakdown in Gases* (Methuen, London, 1957).
- ²J. Dutton, in *Electrical Breakdown in Gases*, edited by J. M. Meek and J. D. Craggs (Wiley Series in Plasma Physics) (Wiley, New York, 1978), Chap. 3, p. 209.
- ³E. E. Kunhardt, *IEEE Trans. Plasma Sci.* **PS-8**, 130 (1980).
- ⁴H. Raether, *Electron Avalanches and Breakdown in Gases* (Butterworths, London, 1964).
- ⁵L. B. Loeb, *Electrical Coronas—Their Basic Physical Mechanisms* (University of California Press, Berkeley, CA, 1965).
- ⁶A. J. Davies, *Proc. IEEE* **133**, 217 (1986).
- ⁷A. J. Davies, C. J. Evans, and P. Townsend, *Proc. IEE* **124**, 179 (1977).
- ⁸K. Yoshida and H. Tagashira, *J. Phys. D* **9**, 435 (1976).
- ⁹J. P. Novak and R. Bartnikas, *J. Appl. Phys.* **62**, 3605 (1987).
- ¹⁰F. Bastien and E. Marode, *J. Phys. D* **18**, 377 (1985).
- ¹¹R. Morrow, *Phys. Rev. A* **32**, 1799 (1985).
- ¹²R. S. Sigmond, in *Electrical Breakdown in Gases*, edited by J. M. Meek and J. D. Craggs (Wiley Series in Plasma Physics) (Wiley, New York, 1978), Chap. 4, p. 319.
- ¹³R. T. Waters, in *Electrical Breakdown in Gases*, edited by J. M. Meek and J. D. Craggs (Wiley Series in Plasma Physics) (Wiley, New York, 1978), Chap. 5, p. 385.
- ¹⁴R. T. Waters, *Proc. IEE* **128**, 319 (1981).
- ¹⁵M. Goldman and R. S. Sigmond, *IEEE Trans. Electr. Insul.* **EI-17**, 90 (1982).
- ¹⁶W. P. Allis, in *Handbuch der Physik, XXI*, edited by S. Flügge (Springer, Berlin, 1956), pp. 383–444.
- ¹⁷D. R. Wilkins and E. P. Gyftopoulos, *J. Appl. Phys.* **37**, 3533 (1966).
- ¹⁸L. E. Kline, *J. Appl. Phys.* **58**, 3715 (1985).
- ¹⁹K. Ramakrishna, Ph.D. thesis (University of Pennsylvania, 1988).
- ²⁰N. N. Lebedev, *Special Functions and their Applications*, translated by R. A. Silverman (Dover, New York, 1972), p. 213.
- ²¹A. von Engel, *Ionized Gases*, 2nd ed. (Oxford University Press, London, 1965), p. 180.
- ²²S. C. Brown, *Basic Data of Plasma Physics, 1966*, 2nd ed. (M. I. T. Press, Cambridge, MA, 1967), p. 182.
- ²³J. Dutton, *J. Phys. Chem. Ref. Data* **4**, 577 (1975).
- ²⁴J. W. Gallagher, E. C. Beatty, J. Dutton, and L. C. Pitchford, *J. Phys. Chem. Ref. Data* **12**, 109 (1983).
- ²⁵E. Hinnov and J. G. Hirschberg, *Phys. Rev.* **125**, 795 (1962).
- ²⁶S. V. Patankar, *Numerical Heat Transfer and Fluid Flow* (Hemisphere, Washington, DC, 1980).
- ²⁷R. G. Fleagle and J. A. Businger, *An Introduction to Atmospheric Physics*, 2nd ed. (International Geophysics Series, Academic, New York, 1980), Vol. 25, pp. 135 and 150.
- ²⁸L. E. Kline, *J. Appl. Phys.* **45**, 2046 (1974).
- ²⁹K. Yoshida and H. Tagashira, *J. Phys. D* **9**, 491 (1976).
- ³⁰I. Abbas and P. Bayle, *J. Phys. D* **13**, 1055 (1976).